Dimerization Affects Collective Dynamics of Triosephosphate Isomerase†

Sertan Cansu and Pemra Doruker*

Department of Chemical Engineering and Polymer Research Center, Bogazici University, Bebek, 34342, Istanbul, Turkey

Received September 20, 2007; Revised Manuscript Received December 4, 2007

ABSTRACT: Molecular dynamics simulations (30−60 ns runs) are performed on free/apo triosephosphate isomerase (TIM) to determine any correlation between collective motions and loop 6 dynamics. Native TIM is reported to be active only as a homodimer even though cooperativity has not been observed between the two identical subunits. Both dimeric and monomeric (isolated from dimer) forms of TIM are simulated in explicit water at 300 K and 1 bar to inspect any differences between the structures in terms of fluctuation dynamics and functionally important loop 6 dynamics/closure. Significant cross-correlations between residue fluctuations are observed in the dimer, which result from the global counter-rotations of the two identical subunits in the essential modes of the dimer. Specifically, the first essential mode contributing to 34% of overall motion of the dimer is strongly coupled to the loop 6's closure over the active site. In contrast, such significant correlations cannot be observed in the monomeric structure, which maintains relatively localized motions of the loops in the essential modes. Thus, the onset of collective motions at ns time scale due to dimerization has functional implications as to the coordination of loop 6 closure.

Protein flexibility and dynamics are crucial for enzyme activity. In many cases binding of ligands to enzymes leads to conformational changes, such as those between the open and closed states of proteins. It is still a challenging and fundamental task to uncover the relationship between an enzyme's activity and dynamics at the molecular level because protein motions cover a broad range of length and time scales (*1*). In this study, we will address the structure−function relationship of the enzyme triosephosphate isomerase (TIM[1]), for which numerous experimental and computational studies exist (*1*−*3*).

TIM is an important enzyme in glycolysis, catalyzing the interconversion between dihydroxyacetone phosphate (DHAP) and D-glyceraldehyde 3-phosphate (GAP). Native TIM is active as a dimer, but no allostery or cooperativity between the identical monomers has been reported (*4*). Each monomer/subunit comprises 248 residues and adopts an $(\alpha/\beta)_8$ fold, commonly named the TIM barrel. In Figure 1a the X-ray structure for the apo form is shown together with the secondary structures in the $(\alpha/\beta)_8$ fold (each consecutive β strand, loop and α-helix are indicated by the same color, such as β1, loop1/L1 and α1 in red). There are three catalytically important residues (shown in magenta and stick representation in Figure 1b) located at the periphery of the β-core region of each TIM barrel: Glu165 and His95 participate in proton transfer, and Lys13 hydrogen bonds weakly with the bridging oxygen of the ligand (*5*). The apo/open (Protein Data Bank, PDB code: 8TIM) and bound/closed (PDB code: 1TPH) structures are aligned in Figure 1b. The ligand in the complex form (shown as black spheres) is phosphoglycolohydroxamate (PGH), an intermediate analogue having the same structure and orientation with the substrate DHAP in the crystal structures (*5*).

Loop 6 is crucial for TIM's catalytic activity in that it closes over the bound ligand and protects it from solvent exposure during reaction (in Figure 1b, dark green, open/apo conformation; dark blue, closed/bound conformation). However, the loop also opens and closes as a natural motion of the enzyme in apo TIM, i.e., it is not ligand-gated (*6*). The highly conserved loop 6 (residues Pro166−Ala176) comprises three hinge residues each at the N- and C-termini and a five residue tip region in between. Mutation of these hinge residues to Gly (excluding Pro166) adversely affects catalysis, resulting in the slowing down of loop motion due to sampling of many more conformations (*7*, *8*).

Other than the two structures shown in Figure 1b, there are many other structures of TIM present in the PDB (*9*). When available X-ray structures are aligned, mainly the conformational flexibility of loop 6 between open and closed states is observed. As a result, molecular dynamics (MD) (*10*−*12*) and Langevin dynamics (*13*) simulation studies have so far concentrated on this loop region without taking the conformational flexibility of the whole protein into account. In contrast to previous simulations, we have recently drawn attention to dominant collective motions of TIM—possibly being coupled to loop opening/closure—revealed by elastic network model analysis of the intact dimeric structure (*14*).

In current work, for the first time—at least to our knowledge—classical MD simulations of appreciable length (30−60 ns) are performed on apo TIM in explicit solvent

† This work was supported by the COSBIOM Project (EU-FP6-ACC-2004-SSA-2 Contract No. 517991), Bogazici University B.A.P. (Project 06A509D) and TUBITAK Project (104M247). S.C. acknowledges TUBITAK-BIDEB SSA-2 Project Fellowship.

* To whom correspondence should be addressed. Mailing address: Department of Chemical Engineering and Polymer Research Center, Bogazici University, Bebek, 34342, Istanbul, Turkey. Phone: +90-212-3597365. Fax: +90-212-2575032. E-mail: doruker@boun.edu.tr.

[1] Abbreviations: TIM, triosephosphate isomerase; DHAP, dihydroxyacetone phosphate; GAP, D-glyceraldehyde 3-phosphate; PGH, phosphoglycolohydroxamate; PDB, Protein Data Bank; MD, molecular dynamics; RMSD, root-mean-square deviation

10.1021/bi701916b CCC: $40.75
Published on Web 01/12/2008

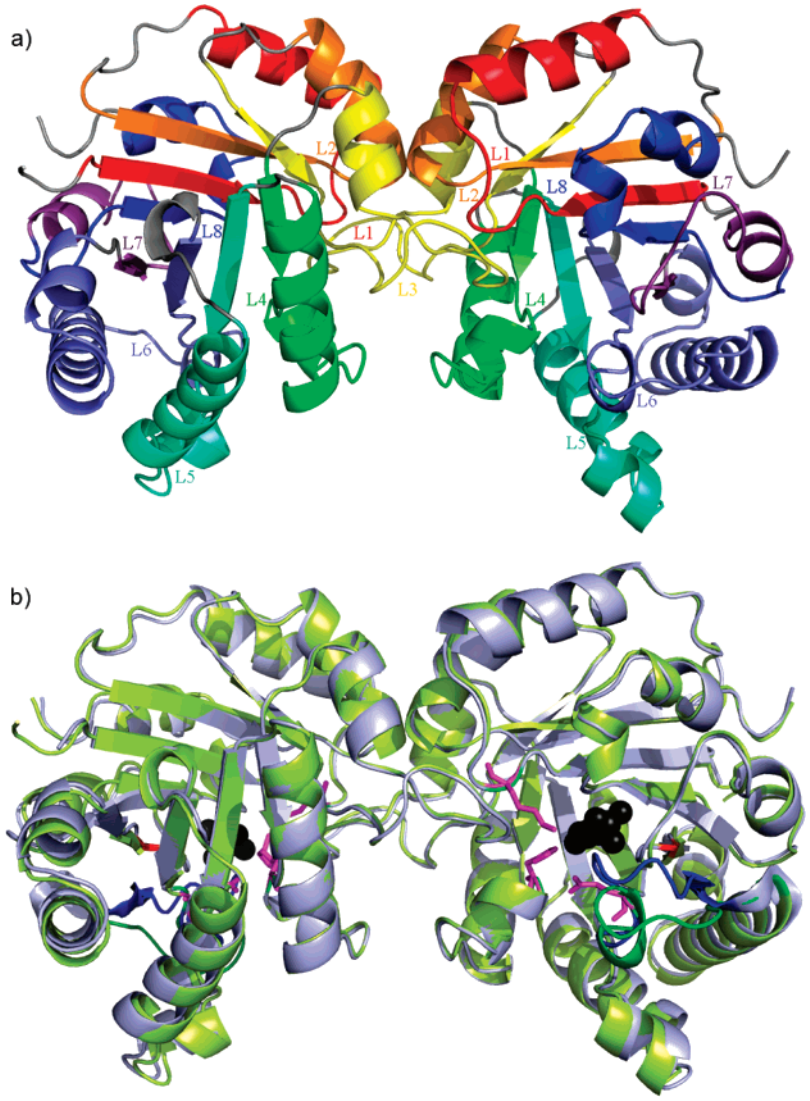

FIGURE 1: X-ray structures of chicken TIM. (a) Apo TIM secondary structures are indicated with each consecutive β strand, loop and α-helix shown in same color. (b) Free (8TIM, light green) and bound (1TPH, light blue) TIM structures are aligned. Active site residues (Lys13, His95 and Glu165) and the inhibitor PGH are shown in magenta and black, respectively. The main difference between free and bound forms is the open and closed conformations of loop 6 indicated in dark green and dark blue, respectively.

without constraining any parts of the protein. Our aim is to extract collective motions and to investigate their correlation with active site loop dynamics. In addition, MD simulations on monoTIM (isolated monomers from dimeric TIM) are carried out in order to observe any changes in equilibrium and dynamic properties of the monomer, which could explain why native TIM is active as a dimer.

MATERIALS AND METHODS

Molecular dynamics simulations were carried out using the program AMBER (*15*, *16*) with the ff03 force field parameters (*17*). We performed three independent runs for apo TIM at 300 K: (i) 60 ns run of the dimer structure (subunits A and B), (ii) 30 ns run of the A subunit, and (iii) 60 ns run of the B subunit. The apo structure of chicken TIM (PDB code: 8TIM) with 2.58 Å resolution is used as the starting conformation for all MD simulations. The simulation details are summarized in Table 1, and the procedure is as follows.

A periodic truncated octahedron box was used for solvation of the protein in explicit TIP3P water molecules (*18*).

Table 1: Simulation System Details

run	simulation length (ns)	box dimension[a] (Å)	total no. of atoms	no. of H_2O molecules	no. of Cl^- ions
dimer	60	107	57,532	16,674	8
monomer A	30	77	23,066	6,437	4
monomer B	60	77	23,066	6,437	4

[a] Truncated octahedron box is used.

Energy minimization was performed using 50 cycles of steepest descent algorithm, followed by conjugate gradient until the RMS gradient per atom reached 0.01 kcal/mol/Å. Each trajectory started with velocity assignments according to the Boltzmann distribution at either 10 or 20 K, and the temperature was gradually raised to 300 K. NPT simulations were performed at 300 K and 1 bar using the weak coupling algorithm for both pressure and temperature (*19*). Constant pressure periodic boundary conditions were used with isotropic position scaling. A time step of 2 fs was used by the implementation of SHAKE algorithm (*20*) for the bonds involving hydrogens. The Ewald summation technique with

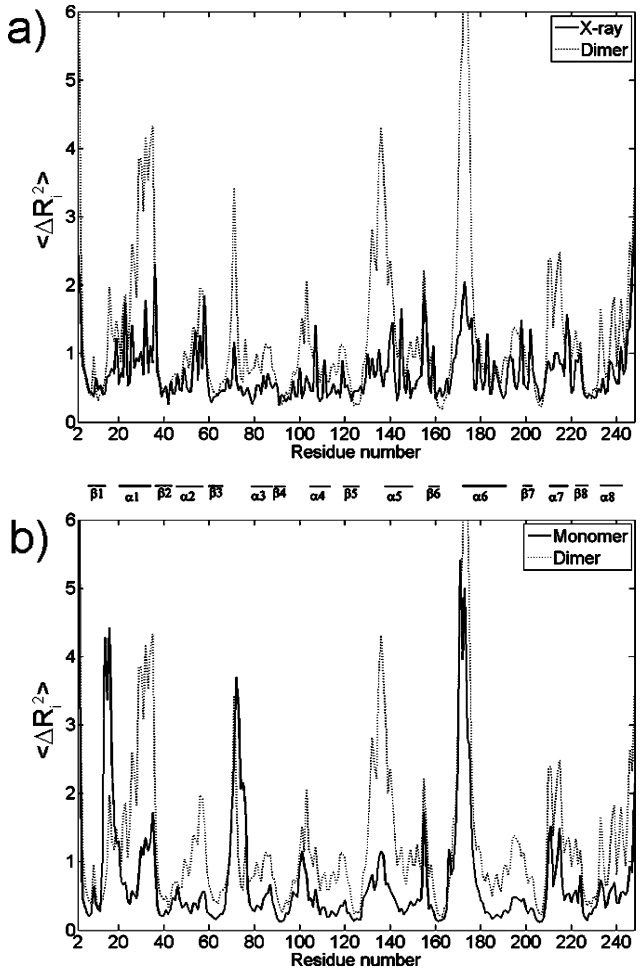

FIGURE 2: Mean square fluctuation (Å^2) about the averege position plotted for C$^\alpha$ atoms of residues. (a) Comparison of X-ray (8TIM-free TIM) and simulation results for dimer, given as an average over identical monomers. (b) Comparison of monomer and dimer runs (averages over A and B monomers in both cases).

the particle-mesh method (*21*) was used to calculate long-range electrostatic interactions with a cutoff distance of 9 Å.

The essential dynamics of TIM (*22*) is extracted from the MD simulation trajectories by using singular value decomposition of the fluctuation matrix. Details of this method and its application can be found in previous work (*23*). The fluctuation matrix is formed based on the C$^\alpha$ atom coordinates of the residues after removal of translational and rotational motions of the protein by aligning each snapshot onto the initial conformation.

RESULTS

Fluctuation Dynamics. The root-mean-square deviation (RMSD) of each snapshot from the initial, energy-minimized structure is calculated after alignment based on C$^\alpha$ atoms (shown in Supporting Information, Figure S1). RMSD values fall within reasonable limits throughout the runs, i.e., less than 2−2.5 Å in monomer and dimer runs. These values denote reliable conformations, which have not deviated extensively from the starting conformation.

In Figure 2a, the mean square fluctuations (MSF) of C$^\alpha$ atoms about their average positions are plotted as function of residue index for the dimer run together with the X-ray data for apo structure (8TIM). The residue fluctuations are averaged over the identical A and B monomers in all cases. In general there is good agreement between simulation and experiment. The loops (particularly loops L5 and L6) and helix α1 exhibit higher fluctuations in solvent environment, i.e., in the absence of crystal contacts.

Figure 2b is a comparison of dimer and monomer simulations, and again results are averages over A and B subunits. Loop 1, which lies at the interface of the dimer and contains the catalytic residue Lys13, becomes highly mobile in isolated monomer simulations. This should have an adverse effect on catalysis, which has been expected in previous protein engineering studies on monomeric TIM and has led to the redesign of loop 1 (*24*). There is a slight broadening of the mobility of loop 3, also forming part of the interface. Deletion of loop 3 has produced a stable monomeric TIM variant with reduced catalytic activity (*25*). Other than these changes at the no-longer-existing interface of the monomer, higher fluctuations are observed predominantly in dimeric structure- α1 and α2, and loop 5 being the most pronounced regions. Almost all helices and loops (excluding L1−L3) show higher fluctuations in dimeric form, the reasons for which will be discussed in upcoming sections. The β-strands forming the core of each TIM barrel fold are at the minima, consistently in experiments and all simulations.

Loop Closure and Dynamics. Three snapshots from dimer (showing the loop of subunit A) and monomer B simulations are displayed in Figure 3a and b, respectively. All the snapshots (green, orange and blue) are aligned with the bound/closed X-ray structure (1TPH), which is also shown in gray. Loop 6 is indicated by darker colors (closed X-ray conformation for loop 6 in black). The snapshots are chosen such that loop 6 can be observed in different conformations: open, intermediate and nearly closed. Green/orange/blue structures represent the snapshots at 7.3/43.3/34.6 ns for the dimer and 2.5/7.6/20.9 ns for the monomer B runs. For example, the tip of loop 6 moves more than 7 Å during loop closure in the dimer (panel a). In Figure 3 panels c and d, four other snapshots are displayed focusing on the loop region from the alternative subunits for dimer and monomer runs, respectively. Specifically, blue/gray/pink/green structures represent the snapshots at 18.6/16.4/12.3/26.4 ns for the dimer run (B chain) and 20.0/4.6/25.6/10.8 ns for the monomer A run. The differences between the dimer and monomer runs can be summarized as follows: Global deformations of the whole protein structure are observed predominantly in the dimer structure. The loop motion seems less targeted between open and closed conformations in the monomer, based on all snapshots sampled (only seven shown in the figure).

To assess the extent of loop closure on a quantitative basis, same as in the work of Massi et al. (*12*), the distances between three residues located at the tip of loop 6 (Ile170, Gly171 and Thr172) and Tyr208 on loop 7 (red residue in Figure 1b) are calculated. The reason for the choice of Thy208 is that it stays quite stationary during the runs (see Figure 2). In Figure 4, these inter-residue distances based on C$^\alpha$ atoms are plotted as a function of time. The dashed and solid horizontal lines represent the distances for the same residue pairs in open (8TIM) and closed (1TPH) X-ray structures, respectively. In the dynamics of dimer structure

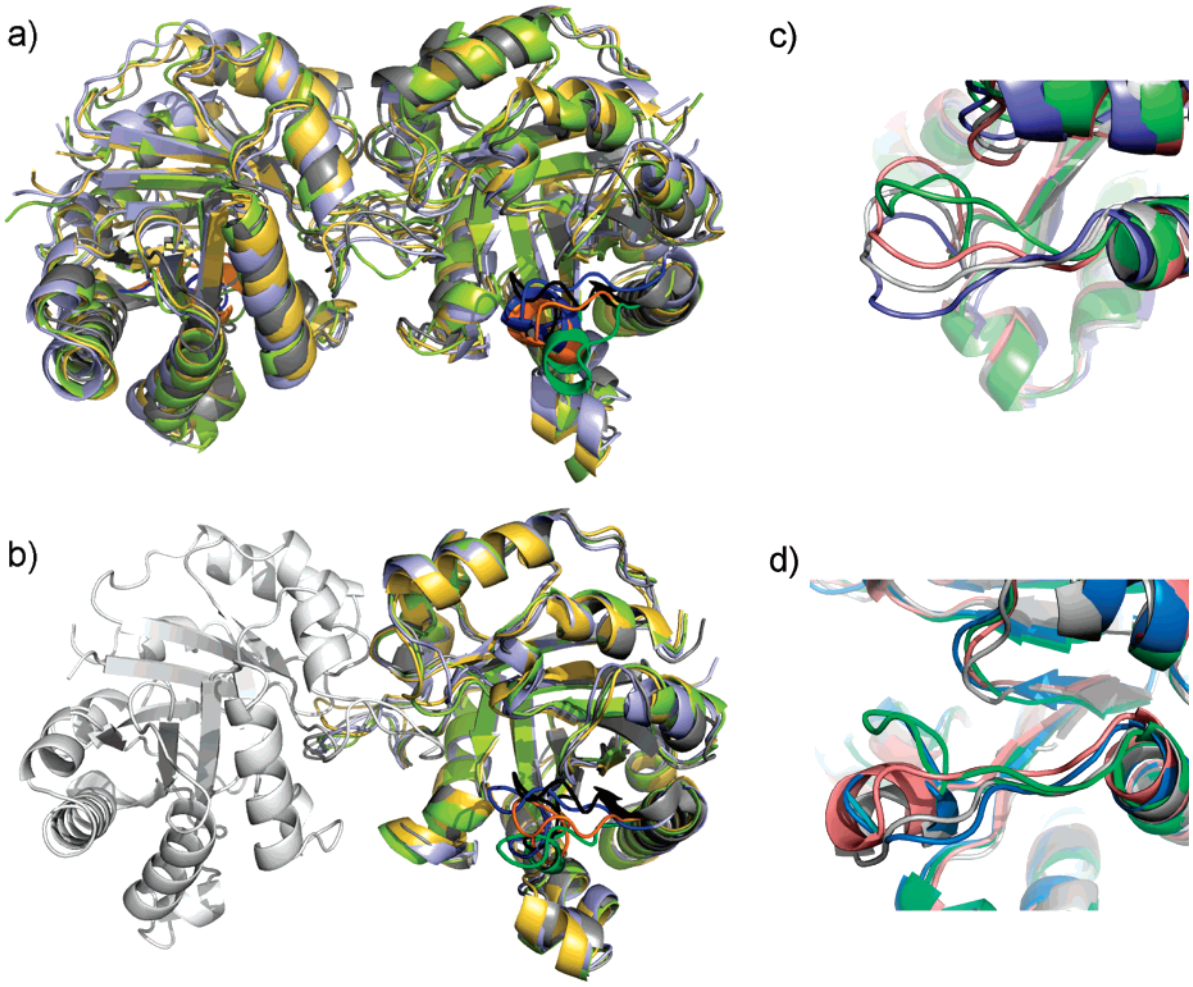

FIGURE 3: Several snapshots obtained from simulations aligned on the X-ray structure (1TPH-bound TIM). (a) Dimer simulation (loop 6 from A chain shown in darker colors), (b) monomer B simulation (loop 6 shown in darker colors), (c) loop 6 conformations from B chain of the dimer, and (d) loop 6 conformations from monomer A simulation. In panels a and b, X-ray structure is shown in gray (loop 6 in black); green, orange and blue are snapshots with the loop in open, intermediate and nearly closed conformations.

(8TIM), snapshots with distances comparable to the closed form are encountered much more frequently than in monomer simulations (specifically looking at black and red lines for residues 170 and 171). In both single chain simulations the loop 6 region tends to remain primarily in open form (dashed lines).

In free TIM, the catalytic residue Glu165 makes hydrogen bonding with Ser96. Upon PGH binding (*5*), Glu165 moves 2−3 Å toward the substrate analogue, assuming the catalytically important conformation. Analysis of our trajectories indicates that the carboxylate oxygens of Glu165 are making hydrogen bonds with either the backbone amide nitrogen or the side-chain hydroxyl group of Ser96 during a significant portion of each run. Specifically, the percentage of snapshots, in which the carboxylate oxygens are hydrogen bonded to Ser96, are 92.7% and 87.9% for dimer and monomer runs, respectively (averaged over A and B chains and the two oxygens in each case). Of course complete closure of the loop and the movement of Glu165 toward the ligand observed in the reference structure (1TPH) necessitates the presence of a ligand, which is not present in our apo structures. Moreover the time scale of loop 6 motion has been found experimentally to be on the order of microseconds (*6*, *8*, *12*, *26*, *27*). As a result we cannot expect to see complete closure and reopening during our runs on the ns scale.

In Figure 5, the surface representation of the closed X-ray structure (1TPH, panel a) is compared with one of the relatively closed snapshots chosen from the dimer (at 34.6 ns, panel b) and monomer B (at 20.9 ns, panels c and d showing two different views of the same snapshot) runs. Loop 6 residues are colored in blue, and active site residues Lys13, His95 and Glu165 are shown in red, green and orange, respectively. The solvent exposure of the active site region in dimer snapshot (panel b) resembles that of the X-ray structure, where the ligand PGH has been removed for comparison of the surfaces. In contrast, in the monomer snapshot Lys13 and His95 are more solvent exposed at the no-longer-existing interface region (panel d).

Another issue is whether loop 6 dynamics resembles that of a rigid lid. This could be determined by looking at the pseudodihedral angles of the loop region, i.e., the internal degrees of freedom of the chain backbone. The *i*th pseudodihedral angle (ϕ_i) connecting residues i and $i + 1$ is calculated by using the C^{α} coordinates of residues $i - 1$, i, $i + 1$ and $i + 2$. Comparison of apo and bound crystal structures has indicated that the loop acts as a rigid body with two hinges, namely, N-terminal hinge located at $\phi_i = 166$, 167, and

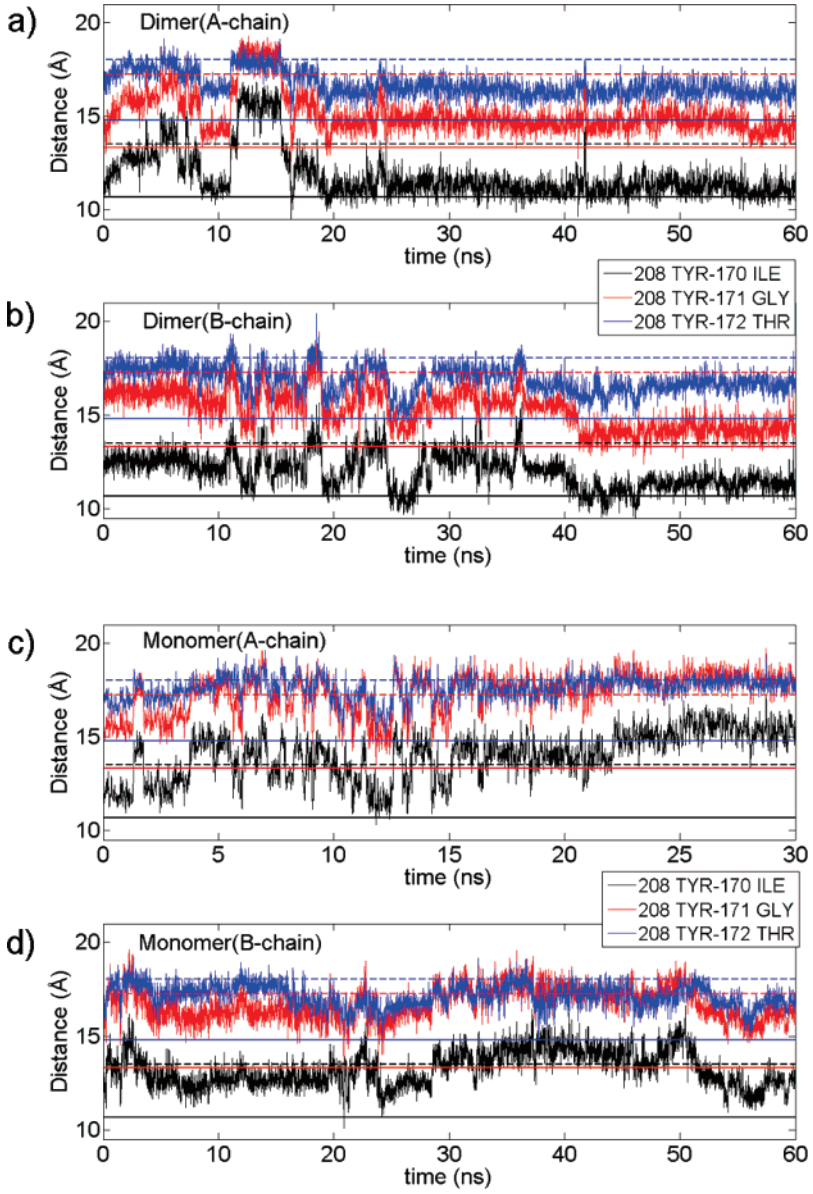

FIGURE 4: Loop opening and closing is observed by plotting the distance between the C^{α} atoms of loop 6 tip residues (black: Ile170, red: Gly171, and blue: Thr172) and Tyr208, which is on loop 7 and displays low mobility in the simulations. The corresponding distances in open (8TIM) and closed (1TPH) X-ray structures are plotted as dashed and solid horizontal lines for reference. In the dynamics of dimer structure (a,b), the closed form is encountered more frequently than the one in monomer simulation (c,d).

C-terminal hinge located at $\phi_i = 174, 175, 176$ (*11*). Recent stochastic boundary MD simulations have shown that rms fluctuations of ϕ_i increase toward the C-terminus of the loop (*12*). Our simulation results given in Figure 6 also confirm that the loop flexibility increases toward the C-terminus on the ns time scale, both for mono- and dimeric TIM with the maximum flexibility observed at the C-terminus hinge. Both curves give RMS fluctuations of ϕ_i averaged over chains A and B, with the monomer and dimer runs showing a similar trend. The increasing trend of fluctuations from the N-terminal to the C-terminal hinge is also consistent with the ns dynamics obtained by solution NMR study (*8*).

Collective Motions Emerging in the Dimer Structure. Figure 7 gives the normalized orientational cross-correlations $C(i,j)$ between residue fluctuations defined as

$$C(i,j) = \frac{\langle \Delta \mathbf{R}_i \cdot \Delta \mathbf{R}_j \rangle}{[\langle \Delta \mathbf{R}_i \cdot \Delta \mathbf{R}_i \rangle \langle \Delta \mathbf{R}_j \cdot \Delta \mathbf{R}_j \rangle]^{1/2}} \qquad (1)$$

where $\Delta \mathbf{R}_i$ is the fluctuation in the position vector $\mathbf{R}_i$ of site i. The brackets represent time averages over recorded snapshots. The cross-correlations vary in the range $[-1, 1]$ with the lower and upper limits indicating fully anticorrelated and correlated fluctuations in terms of orientation, respectively. $C(i,j) = 0$ gives uncorrelated fluctuations in terms of orientation. In the dimer simulation (Figure 7a) there are strong positive and negative correlations, both within each subunit (intra-subunit, squares on the diagonal) and between different subunits (inter-subunit, off-diagonal). These distinct regions with high $+/-$ correlations are indicative of collective domain motions that dominate the overall dynamics of the dimer. In contrast, such strong correlations cannot be observed in single monomer A and B (Figure 7b and c) simulations. We should state that the level and pattern of correlations that emerge from TIM dimer simulation are very significant compared to previous MD results of ns duration, such as on *Eco*RI−DNA complex (*28*).

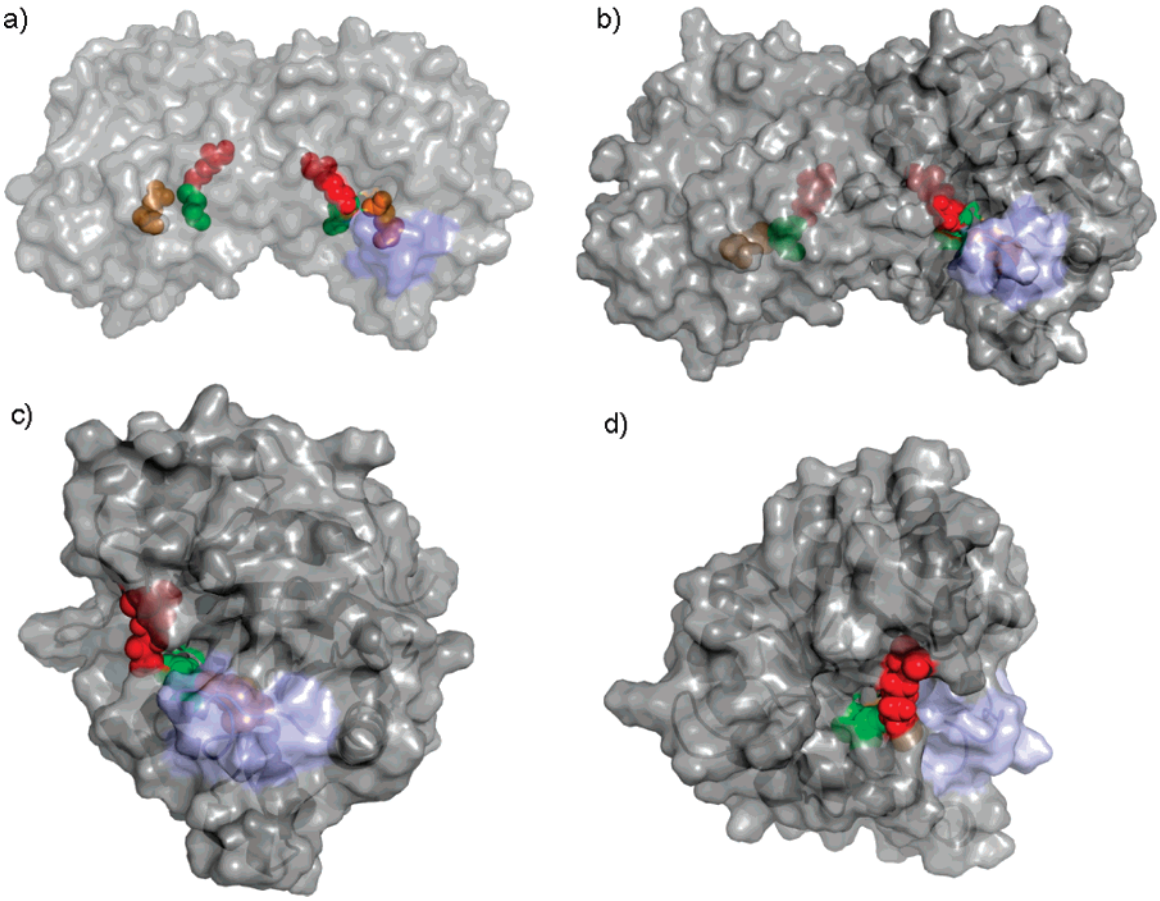

FIGURE 5: Surface representations of (a) closed X-ray structure (1TPH) with the inhibitor PGH removed from the binding pocket, (b) a relatively closed snapshot from dimer simulation (at 34.6 ns) and (c) a snapshot from monomer B simulation (at 20.9 ns). (d) The snapshot from monomer simulation is rotated around by about 45°. Blue regions stand for the loop 6 (residues 166−176). The active site residues—Lys13, His95 and Glu165—are shown in red, green and orange, respectively. The solvent exposure of the dimer resembles that of the X-ray structure without PGH, whereas Lys13 and His95 in monomer B are relatively more solvent exposed due to the absence of the second monomer.

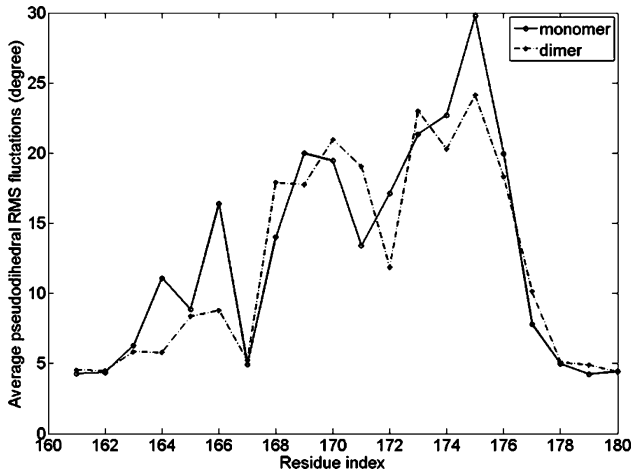

FIGURE 6: RMS fluctuations of pseudodihedral angles as a function of residue number for the region encompassing loop 6. The torsional angle for the *i*th residue is based on the C^{α} coordinates of residues $i-1$, i, $i+1$ and $i+2$. RMS fluctuations are averaged over the loops in the dimer and over the two independent runs for the monomer case. The loop in both cases acts as a flexible rather than a rigid lid.

Based on symmetry considerations, it is expected that dimerization should give rise to rigid body motions of the two monomers, which may, in turn, be crucial for enzymatic activity. To get a better insight about the cooperative dynamics in the structure, we will look at the cross-correlations based on the first five modes extracted by singular value decomposition. The five modes that form the essential subspace (*22*) constitute 58%, 39% and 42% of the overall motion in dimer, monomer A and monomer B runs, respectively. Figure 8 gives the cross-correlations in the essential subspace of these runs, specifically (a) intra-subunit (dimer), (b) inter-subunit (dimer) and (c) monomer (averaged over A and B). Since the correlation patterns are quite similar for A and B chains in the dimer, the cross-correlations have been averaged over the two chains in the dimer. The strongly correlated (red) and anticorrelated (blue) regions resulting from the collective motions are clearly observed. Even though some negatively correlated and few positively correlated regions appear in monomer simulations, they are not as noteworthy as in the dimeric structure. Clearly there is a core region/domain that runs across the interface of the dimer. This core region is made up of positively correlated residues ~45−125 from both chains A and B, i.e., including intra-subunit and inter-subunit interactions. This region comprises the residues starting from α2 running to the end of β5 together with loops 3 and 4.

Figure 9 shows the first mode deformations in dimer and monomer B runs. A global twisting motion of the two monomers in opposite directions can be observed in panel a. There is a separate rotation axis for each monomer that passes through the core of each TIM barrel. The two axes are not aligned due to accompanying bending motion of the

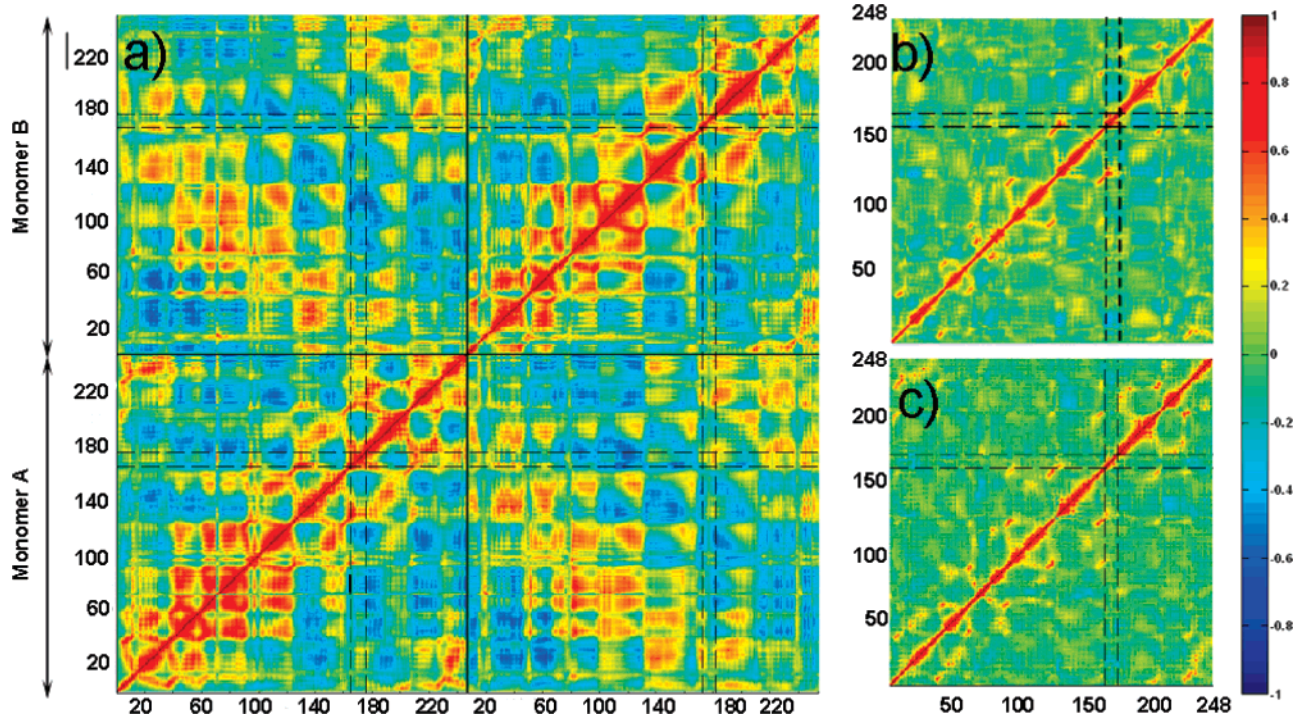

FIGURE 7: Normalized cross-correlations between residue fluctuations (eq 1) including all modes. Strong positive and negative correlations are observed in the (a) dimer compared to relatively localized correlations in (b) monomer A and (c) monomer B.

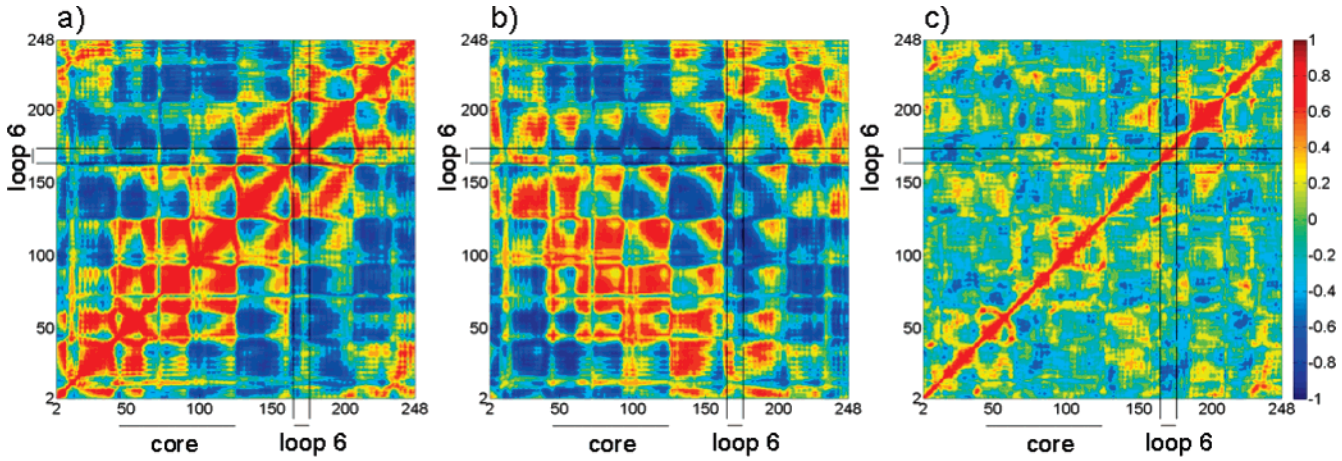

FIGURE 8: Normalized cross-correlations between residue fluctuations in the first five essential modes (averages over A and B chains). (a) Intra-subunit correlations for dimer, (b) inter-subunit correlations for dimer, and (c) correlations for monomer runs.

monomers. In contrast, the first mode of the monomer describes independent—not globally coordinated—deformations of the loops (panel b). Two alternative conformations given in panels c and d depict the loop motion resulting from first mode. Partial loop closure is observed in the dimer (the tip residue Thr172 moves about 5.6 Å, Figure 9c), whereas the loop motion is along the lateral direction in the monomer (tip movement of 2.0 Å, Figure 9d), i.e. not along loop closure. In other essential modes, such as second, third and fourth modes (not shown), similar counter-rotation-type motion with different axes is observed in the dimer. These collective motions are also consistent with our previous elastic network results (*14*).

At this point we need to make a comment based on the recent work by Van Wynsberghe and Cui (*29*), where they have stated that a large number of low-frequency normal modes are necessary for identification of correlated motions using residue cross-correlations. In contrast to the case of harmonic normal modes, a small number of anharmonic modes extracted from MD simulations can describe a very high percentage of the protein motion. As stated above, the first five modes describe ~60% of the overall motion in the dimer and ~40% in the monomer runs. However, if we perform a coarse-grained normal-mode analysis of TIM as in our previous work (*14*), we need to include ~50 (~140) modes to describe at least 30% (40%) of the overall motion. In general it is expected that correlations should get weaker as more modes are included; still, the correlation plots based on all modes (Figure 7) and on five modes (Figure 8) exhibit very similar features. Thus, it seems justified to focus on the first five essential modes in our case.

Correlation between Collective Motions and Loop Dynamics. For each essential (or principal) mode, the overlap values are calculated by taking the dot product of eigenvectors for the tip region (169A−173G) of loop 6 with the deformation vector that is in the direction of loop closure.

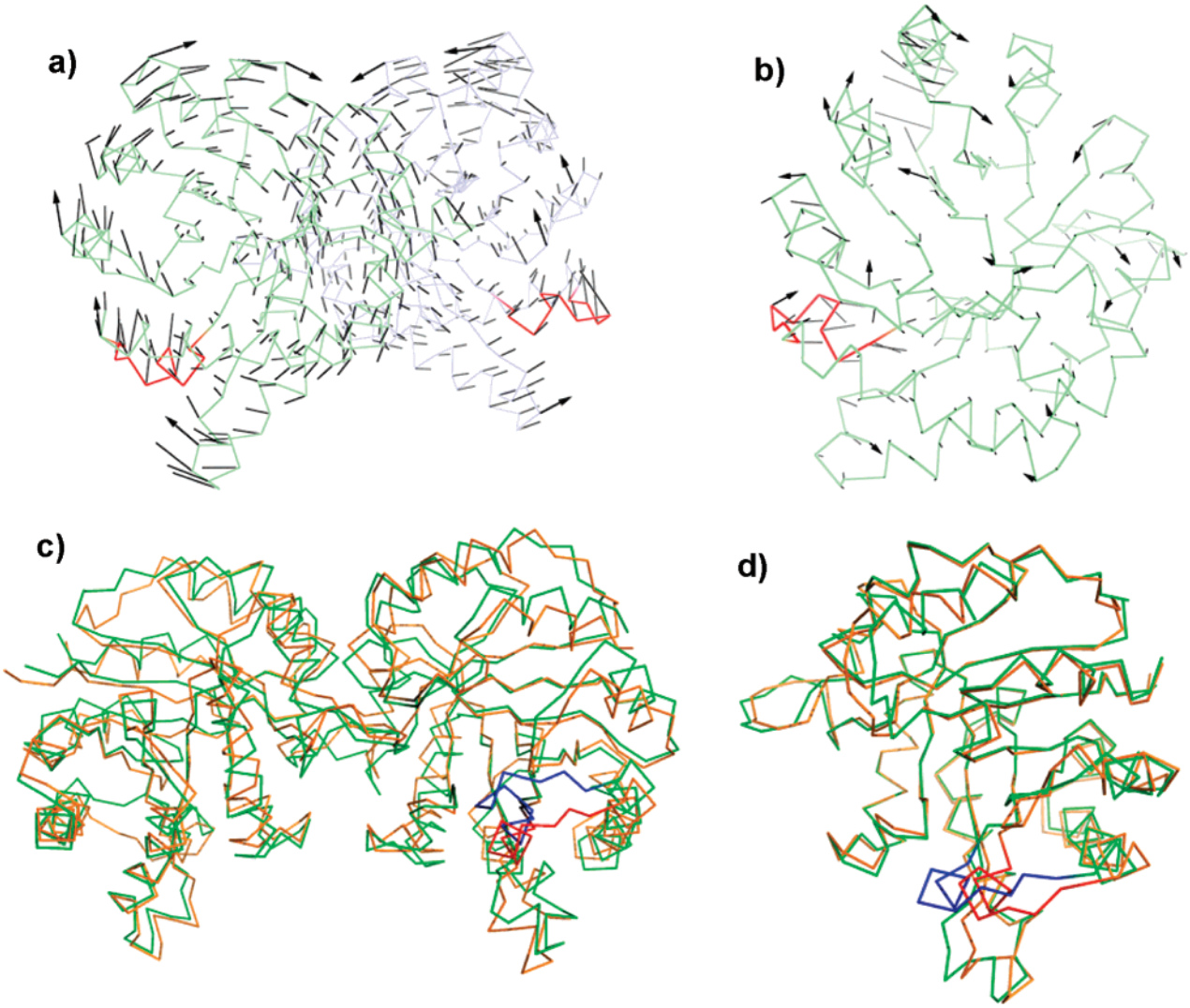

FIGURE 9: Deformations in the first essential mode. (a) Looking from a different point of view, the counter-rotation movement of the subunits is indicated by deformation vectors. The arrows show the directions of movement for selected residues. This collective motion in dimer assists loop closure (red). (b) A dominant collective motion cannot be observed in the first mode of monomer simulation. (c) Two different conformations (green and yellow) from the dimer simulation. Based on these snapshots indicating loop closure (red and blue), the tip residue Thr172 moves about 5.6 Å. (d) Conformations from monomer B exhibit a lateral motion of the loop (red and blue), rather than closure.

Table 2: Overlap of the Loop's Motion with the Loop Closure Direction in the Essential Modes[a]

	monomer A		monomer B		dimer		
modes	overlap (A)	mode contribution	overlap (B)	mode contribution	overlap (A chain)	overlap (B chain)	mode contribution
1	0.22	0.13	0.07	0.17	**0.86**	**0.67**	0.34
2	0.08	0.09	**0.60**	0.09	0.35	0.20	0.09
3	0.24	0.07	**0.63**	0.08	**0.62**	0.14	0.08
4	0.31	0.06	0.30	0.05	**0.80**	**0.82**	0.04
5	0.25	0.04	**0.71**	0.04	**0.86**	0.34	0.03

[a] The overlap values between loop displacement observed in specific modes and the displacement between open and closed X-ray conformations is calculated for the tip region residues 169−173. The contribution of each essential mode to the overall motion is given.

The deformation vector is calculated based on aligned open (8TIM) and closed (1TPH) X-ray structures, again for the specified tip residues of loop 6. In Table 2, the overlap values are tabulated for the first five principal modes, together with the contribution of each mode to the overall motion. In single chain dynamics (monomer A or B) overlap values are lower than the ones in dimeric structure. Overlap values close to one are indicative of similar conformational changes to those observed in crystal structures, and values above 0.6 are highlighted in the table. Specifically, the first mode of dimer contributing to 34% of overall motion exhibits high overlap values (A chain, 0.86; B chain, 0.67). Thus first mode describes strong coupling between the collective motions of TIM and loop opening/closing. In contrast, high values are observed for modes 2, 3 and 5 only in monomer B, but the contribution of these modes to the overall motion is comparatively lower, each being less than 10%.

Figure 10 gives the normalized probability of snapshots along the open/closed transition coordinate for loop 6. Calculations are based on the distance between the tip of loop 6 (Gly171) and Tyr208 (same as the red lines in Figure 4). The corresponding distance in closed (1TPH) X-ray structure is 13.3 Å. First and second row panels refer to the loop conformations in subunit A and B for the dimer run, respectively. For comparison, third and fourth rows belong to monomer runs A and B. Panels in the first, second and

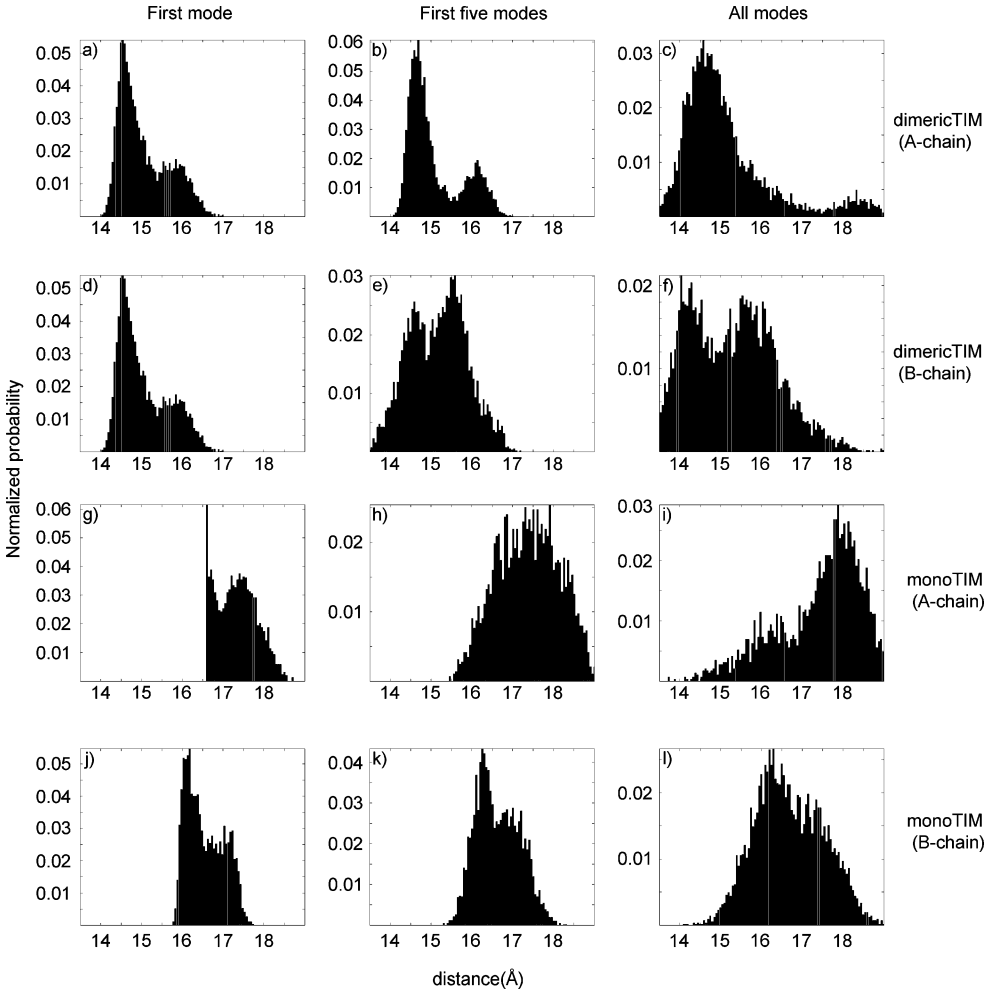

FIGURE 10: Normalized probability distribution of the open/closed transition coordinate based on the distance between Tyr208 and Gly171 (the tip of loop 6). Panels in the first (a, b, c), second (d, e, f), third (g, h, i) and fourth (j, k, l) rows give the distributions for chain A in dimer run, chain B in dimer run, monomer A and monomer B runs, respectively. Panels in the first column (a, d, g, j) and in the second column (b, e, h, k) are based on the first essential mode of PCA and the cumulative action of the first five essential modes, respectively. The last column (panels c, f, i, l) indicates overall motion, i.e., all modes. The corresponding distances in open (8TIM) and closed (1TPH) X-ray structures are 17.3 and 13.3 Å, respectively.

third columns refer to the first mode, the cumulative effect of first five modes and the overall motion, respectively. In the first mode, the loops can make significant progress toward closure only in the dimeric structure. A similar trend is observed based on the cumulative action of first five modes (second column). For comparison, the progress toward closure is presented for the overall motion—all modes—as extracted from Figure 4. In summary, the loop closure is to a great extent facilitated by the collective motions in dimeric TIM. This could be one of the reasons—overlooked so far—why native TIM is catalytically active as a dimer.

Finally, loop motion in the different subunits is positively correlated in the essential modes, which is observed in the inter-subunit orientational correlation plot for the dimer (Figure 8b). Normalized cross-correlations, $C(i,j)$, for the loop residues from different subunits are listed in Table 3 for the first mode and the cumulative first five modes. Specifically, loop residues, excluding the N-terminal hinge residues and 171, exhibit high positive correlations in the cumulative first five modes.

Table 3: Inter-Subunit Cross-Correlation Values for the Loop Residues in the First Mode and for the First Five Modes

residues from chains A and B	cross-correlations	
	first mode	first five modes
166	−0.2357	0.1768
167	−0.3677	−0.2058
168	−0.2524	−0.0322
169	0.1807	0.6488
170	0.4531	0.8866
171	−0.1791	−0.2938
172	0.2893	0.7683
173	0.3902	0.6496
174	0.5528	0.8451
175	0.5025	0.9482
176	0.4122	0.802

DISCUSSION

Native TIM is active as a dimer, even though no cooperativity has been reported between the two active sites (*4*). Dimers of identical subunits—the simplest form of protein aggregates—have been studied extensively by Weber and co-workers via dissociation into monomers using hydrostatic pressure (*30*−*32*). These studies have aimed at the determination of energetics, dynamics and structural features of the equilibrium between dimeric and monomeric forms of proteins, such as rubilose biphosphate carboxylase (*30, 31*). In this study, we have analyzed at the molecular

scale the differences in equilibrium and dynamics properties of monomeric and dimeric forms of TIM.

Molecular simulations on TIM have so far concentrated on the dynamics of active site and loop 6 (*10*−*13*). In contrast, our recent study with elastic network models (*14*) has shown the existence of dominant domain motions in TIM with functional importance. Accordingly, conformational freedom of the whole apo TIM structure has been taken into account for the first time in our current MD simulations, both for monomeric and for dimeric TIM. In conformity with elastic network model results, significant collective motions are observed in the essential modes describing the counter-rotation of the identical subunits in the dimer (Figure 9). In contrast, monoTIM structure displays rather independent dynamics of the outer loops without major cooperative deformations in the whole monomer. More importantly, the global twisting in the first mode of dimer simulation that accounts for 34% of total motion is strongly coupled to the loop 6 dynamics along the loop closure direction, whereas no such action is observed in monoTIM.

Figure 10 clearly indicates that loop 6 makes significant progress toward closure based on the action of essential modes—most importantly the first mode—in the dimeric structure. Thus, the effective coordination of loop 6 by the global motions in apo TIM emerges as an inherent feature of the native enzyme. A recent NMR relaxation study (*33*) has shown similar characteristic motions of cyclophilin A during catalysis and in apo form, indicating that the intrinsic nature of collective dynamics may affect the catalytic turnover rate.

As has been expected in previous work on monomeric TIM (*24*), our simulations also show that the absence of the second subunit in monoTIM increases solvent exposure of active site residues (Lys13 and His95 in Figure 5), which should negatively affect catalytic activity. At the same time, the onset of rigid-body motions—predominantly twisting—of the two monomers in dimeric TIM has functional importance in terms of targeting loop 6's closure over the active site, which is not observed in monoTIM in the time scale of our simulations. Thus, dimeric TIM captures the features of a functional scaffold, which controls the motion of outer helices and loops about the β-strand core region of each barrel. Since closure of loop 6 over the active site is necessary for catalysis, its proper coordination should—at least to some extent—contribute to the high catalytic efficiency of TIM.

ACKNOWLEDGMENT

We thank Bulent Balta and Ozge Kurkcuoglu for helpful discussions. S.C. thanks Aysegul Ozen for the technical support.

SUPPORTING INFORMATION AVAILABLE

RMS of the snapshots from the initial energy-minimized structure for dimer and monomer runs are given in Figure S1. This material is available free of charge via the Internet at http://pubs.acs.org.

REFERENCES

1. Daniel, R. M., Dunn, R. V., Finney, J. L., and Smith, J. C. (2003) The role of dynamics in enzyme activity, *Annu. Rev. Biophys. Biomol. Struct. 32*, 69−92.
2. Wang, W., Donini, O., Reyes, C. M., and Kollman, P. A. (2001) Biomolecular simulations: recent developments in force fields, simulations of enzyme catalysis, protein-ligand, protein-protein, and protein-nucleic acid noncovalent interactions, *Annu. Rev. Biophys. Biomol. Struct. 30*, 211−243.
3. Benkovic, S. J., and Hammes-Schiffer, S. (2003) A perspective on enzyme catalysis, *Science 301*, 1196−1202.
4. Schnackerz, K. D., and Gracy, R. W. (1991) Probing the catalytic sites of triosephosphate isomerase by ^{31}P-NMR with reversibly and irreversibly binding substrate analogs, *Eur. J. Biochem 199*, 231−238.
5. Zhang, Z., Sugio, S., Komives, E. A., Liu, K. D., Knowles, J. R., Petsko, G. A., and Ringe, D. (1994) Crystal structure of recombinant chicken Triosephosphate isomerase-Phosphoglycolohydroxamate complex at 1.8Å resolution, *Biochemistry 33*, 2830−2837.
6. Williams, J. C., and McDermott, A. E. (1995) Dynamics of the flexible loop of triosephoshate isomerase: the loop motion is not ligand gated, *Biochemistry 34*, 8309−8319.
7. Xiang, J., Jung, J., and Sampson, N. S. (2004) Entropy effects on protein hinges: the reaction catalyzed by triosephosphate isomerase, *Biochemistry 43*, 11436−11445.
8. Kempf, J. G., Jung, J. Y., Ragain, C., Sampson, N. S., and Loria, J. P. (2007) Dynamic requirements for a functional protein hinge, *J. Mol. Biol. 368*, 131−149.
9. Berman, H. M., Westbrook, J., Feng, Z., Gilliland, G., Bhat, T. N., Weissig, H., Shindyalov, I. N., and Bourne, P. E. (2000) The Protein Data Bank, *Nucleic Acids Res. 28*, 235−242.
10. Brown, F. K., and Kollman, P. A. (1987) Molecular dynamics simulations of "loop closing" in the enzyme triose phosphate isomerase, *J. Mol. Biol. 198*, 533−546.
11. Joseph, D., Petsko, G. A., and Karplus, M. (1990) Anatomy of a conformational change: hinged lid motion of the triosephosphate isomerase loop, *Science 249*, 1425−1428.
12. Massi, F., Wang, C., and Palmer, A. G., III (2006) Solution NMR and computer simulation studies of active site loop motion in triosephosphate isomerase, *Biochemistry 45*, 10787−10794.
13. Derreumaux, P., and Schlick, T. (1998) The loop opening/closing motion of the enzyme triosephosphate isomerase, *Biophys. J. 74*, 72−81.
14. Kurkcuoglu, O., Jernigan, R. L., and Doruker, P. (2006) Loop motions of triosephosphate isomerase observed with elastic networks, *Biochemistry 45*, 1173−1182.
15. Case, D. A., Darden, T. A., Cheatham, T. E. I., Simmerling, C. L., Wang, J., Duke, R. E., Luo, R., Merz, K. M., Wang, B., Pearlman, D. A., et al. (2004) AMBER 8, University of California, San Francisco.
16. Case, D. A., Cheatham, T. E., Darden, T., Gohlke, H., Luo, R., Merz, K. M., Jr., Onufriev, A., Simmerling, C., Wang, B., and Woods, R. (2005) The Amber biomolecular simulation programs, *J. Comput. Chem. 26*, 1668−1688.
17. Duan, Y., Wu, C., Chowdhury, S., Lee, M. C., Xiong, G., Zhang, W., Yang, R., Cieplak, P., Luo, R., and Lee, T. (2003) A Point-Charge Force Field for Molecular Mechanics Simulations of Proteins, *J. Comput. Chem. 24*, 1999−2012.
18. Jorgensen, W. L., Chandrasekhar, J., Madura, J. D., Impey, R. W., and Klein, M. L. (1983) Comparison of simple potential functions for simulating liquid water, *J. Chem. Phys. 79*, 926−935.
19. Berendsen, H. J. C., Postma, J. P. M., Van Gunsteren, W. F., DiNola, A., and Haak, J. R. (1984) Molecular dynamics with coupling to an external bath, *J. Chem. Phys. 81*, 3684−3690.
20. Ryckaert, J. P., Ciccotti, G., and Berendsen, H. J. C. (1977) Numerical integration of the Cartesian equations of motion of a system with constraints: Molecular dynamics of n-alkanes, *J. Comput. Phys. 23*, 327−341.
21. Essman, U., Perera, L., Berkowitz, M. L., Darden, T. A., Lee, H., and Pedersen, L. G. (1995) A smooth Particle Mesh Ewald method, *J. Chem. Phys. 103*, 8577−8593.
22. Amadei, A., Linssen, A. B. M., and Berendsen, H. J. C. (1993) Essential dynamics of proteins, *Proteins 17*, 412−425.
23. Doruker, P., Atilgan, A. R., and Bahar, I. (2000) Dynamics of Proteins Predicted by Molecular Dynamics Simulations and Analytical Approaches: Application to alpha-Amylase Inhibitor, *Proteins 40*, 512−524.
24. Thanki, N., Zeelen, J. P., Mathieu, M., Jaenicke, R., Abagyan, R. A., Wierenga, R. K., and Schliebs, W. (1997) Protein engineering with monomeric triosephosphate isomerase (monoTIM): the

modeling and structure verification of a seven-loop residue, *Protein Eng. 10*, 159−167.
25. Borchert, T. V., Abagyan, R., Jaenicke, R., and Wierenga, R. K. (1994) Design, creation, and characterization of a stable, monomeric triosephosphate isomerase, *Proc. Natl. Acad. Sci. U.S.A. 91*, 1515−1518.
26. Rozovsky, S., McDermott., and A. E. (2001) The Time scale of the Catalytic Loop Motion in Triosephosphate Isomerase, *J. Mol. Biol. 310*, 259−270.
27. Desamero, R., Rozovsky, S., Zhadin, N., McDermott, A., and Callender, R. (2003) Active site loop motion in Triosephosphate Isomerase: T-jump relaxation spectroscopy of thermal activation, *Biochemistry 42*, 2941−2951.
28. Doruker, P., Nilsson, L., and Kurkcuoglu, O. (2006) Collective dynamics of EcoRI-DNA complex by elastic network model and molecular dynamics simulations, *J. Biomol. Struct. Dyn. 24*, 1−15.
29. Van Wynsberghe, A. W., and Cui, Q. (2006) Interpreting correlated motions using normal mode analysis, *Structure 14*, 1647−1653.
30. Erijman, L., Lorimer, G. H., and Weber, G. (1993) Reversible dissociation and conformational stability of dimeric ribulose biphosphate carboxylase, *Biochemistry 32*, 5187−5195.
31. Erijman, L., Paladini, A. A., Lorimer, G. H., and Weber, G. (1993) Plurality of protein conformations of ribulose- 1,5- biphosphate carboxylate oxygenase monomers probed by high-pressure electrophoresis, *J. Biol. Chem. 268*, 25914−25919.
32. Weber, G. (1992) *Protein Interactions*, Chapman & Hall, Inc., New York.
33. Eisenmesser, E. J., Millet, O., Labeikovsky, W., Korzhnev, D. M., Wolf-Watz, M. Bosco, D. A., Skalicky, J. J., Kay, L. E. and Kern, D. (2005) Intrinsic dynamics of an enzyme underlies catalysis, *Nature 438*, 117−121.

BI701916B